Published in final edited form as:
Dev Biol. 2010 November 15; 347(2): 247–257. doi:10.1016/j.ydbio.2010.08.005.

FLN-1/Filamin is Required for Maintenance of Actin and Exit of Fertilized Oocytes from the Spermatheca in *C. elegans*

Ismar Kovacevic and **Erin J. Cram***
Department of Biology, Northeastern University, 134 Mugar Hall, 360 Huntington Ave, Boston, MA 02115

Abstract

Filamin, known primarily for its actin cross-linking function, is a stretch-sensitive structural and signaling scaffold that binds transmembrane receptors and a wide variety of intracellular signaling proteins. The *C. elegans* filamin ortholog, FLN-1, has a well conserved overall structure, including an N-terminal actin-binding domain, and a series of 20 immunoglobulin (Ig)-like repeats. FLN-1 partially colocalizes with actin filaments in spermathecal and uterine cells. Analysis of phenotypes resulting from a deletion allele and RNAi depletion indicates FLN-1 is required to maintain the actin cytoskeleton in the spermatheca and uterus, and to allow the exit of embryos from the spermatheca. FLN-1 deficient animals accumulate embryos in the spermatheca, lay damaged and unfertilized eggs, and consequently exhibit dramatically reduced brood sizes. The phospholipase PLC-1 is also required for the exit of embryos from the spermatheca, and analysis of doubly mutant animals suggests that PLC-1 and FLN-1 act in the same pathway to promote proper transit of embryos from the spermatheca to the uterus. Given the modular protein structure, subcellular localization, genetic interaction with PLC-1, and known mechanosensory functions of filamin, we postulate that FLN-1 may be required to convert mechanical information about the presence of the oocyte into a biochemical signal, thereby allowing timely exit of the embryo from the spermatheca.

Keywords

Filamin; FLN-1; Ovulation; Spermatheca; Actin; PLC-1

Introduction

Filamins are large, dimeric proteins composed of an N-terminal actin-binding domain (ABD) and multiple C-terminal immunoglobulin (Ig)-like filamin repeats (Gorlin et al., 1990). The final Ig-like domain mediates dimerization (Himmel et al., 2003; Stossel et al., 2001). The ABD consists of two tandem calponin homology domains. Human filamins contain 24 Ig-like domains segregated into two rod domains (rod 1 and 2) and connected by flexible hinges (hinge 1 and 2). Although much work has been done to understand the structure and function of filamin, surprisingly little is known about the mechanism by which filamin functions *in vivo*. In *Drosophila melanogaster* the filamin ortholog *cheerio* is required for proper maintenance of ovarian ring canals (Li et al., 1999; Sokol and Cooley,

*All correspondence should be addressed to: Erin J. Cram, Ph.D., Telephone: 617-373-7533, Fax: 617-373-3724, e.cram@neu.edu.

2003), and the *Dictyostelium discoideum* filamin is required for photosensory signaling (Annesley et al., 2007). A number of cell migration (Fox et al., 1998), muscle (Ferrer and Olive, 2008), and bone (Stefanova et al., 2005) disorders have been linked to filamin mutations in humans. Similarly, filamin mutations in mice result in a wide variety of defects, including bone and microvasculature defects (Hart et al., 2006; Zhou et al., 2007).

Filamins organize the actin cytoskeleton into an elastic three-dimensional network and connect the cytoskeleton to transmembrane proteins, including integrins (Calderwood et al., 2001). Additionally, filamins interact with many intracellular signaling proteins, such as migfilin, FilGAP, Trio and small GTPases (Feng and Walsh, 2004; Popowicz et al., 2006). Experimental evidence suggests that filamins may act as mechanical stress sensors (Gehler et al., 2009; Kainulainen et al., 2002; Shifrin et al., 2009; Stossel et al., 2001). Because filamins can concurrently bind transmembrane proteins, filamentous actin, and intracellular signaling components, they are ideally placed to regulate the response of cells or tissues to changing mechanical forces. Filamin may transduce mechanical signals through stretch-sensitive changes in conformation or arrangement of its Ig-like domains that reveal cryptic binding sites for downstream effectors (Nakamura et al., 2007).

The *C. elegans* gonad, essentially consisting of a contractile tube, is an ideal model system for *in vivo* study of filamin function. The *C. elegans* gonad consists of two symmetrical, U-shaped arms connected by a common uterus (Hubbard and Greenstein, 2000; McCarter et al., 1997; Strome, 1986). Germ cells proliferate in the distal gonad, and mature into oocytes as they move proximally. The gonad is enveloped by an outer basal lamina, and most portions of the gonad are surrounded by a layer of contractile, myoepithelial sheath cells (Strome, 1986). The proximal gonad is connected to the spermatheca, which serves as the site of sperm storage and fertilization. The spermatheca consists of three distinct regions: the distal constriction, a central bag-like chamber, and the spermatheca-uterine (sp-ut) valve (McCarter et al., 1997; Strome, 1986).

During each ovulatory cycle, the most proximal oocyte is ovulated into the spermatheca, fertilized, and then released into the uterus (McCarter et al., 1999). Ovulation requires the coordination of signaling between the sperm, oocyte, proximal sheath cells, and the distal spermatheca. Major Sperm Protein (MSP), secreted by the sperm, promotes sheath cell contractions and oocyte meiotic maturation (Miller et al., 2001). Ovulation begins with intense sheath cell contractions and concomitant dilation of the distal spermatheca. The distal spermatheca is pulled over the proximal oocyte, and the oocyte passes through the distal spermathecal constriction to enter the spermatheca, where fertilization occurs immediately (McCarter et al., 1999). Following fertilization, the embryo exits the spermatheca via the sp-ut valve. Oocyte entry is controlled by LIN-3/EGF signaling from the oocyte to the sheath and the distal spermatheca (Clandinin et al., 1998). In the sheath and spermatheca, the LET-23/EGF receptor likely activates PLC-3/Phospholipase C-γ, which generates IP_3 causing release of Ca^{2+} by the ITR-1/IP_3 receptor (Clandinin et al., 1998; Yin et al., 2004). The IP_3 signal is negatively regulated by IPP-5/inositol 5-phosphatase and LFE-2/inositol (1,4,5) trisphosphate-3-kinase (Bui and Sternberg, 2002; Clandinin et al., 1998). Ca^{2+} release is thought to control the contraction of the sheath cells and dilation of the distal spermatheca. With the exception of the role of PLC-1, very little is known about the molecular events that control the exit of embryos from the spermatheca (Kariya et al., 2004).

In this study, we demonstrate that FLN-1/filamin plays a critical structural and mechanosensory role in the *C. elegans* somatic gonad. Using RNAi depletion and analysis of a deletion allele, *fln-1(tm545)*, we demonstrate that loss of *fln-1* results in severe spermathecal exit defects and a dramatically reduced brood size. The expression pattern and

phenotypic analysis show *fln-1* is required in the spermatheca for normal release of embryos and for maintenance of the actin cytoskeleton in the spermatheca and uterus. Interestingly, our analysis suggests that in addition to its structural role in the gonad, filamin may play a role in phosphatidylinositol signaling.

Results

fln-1 encodes three protein isoforms

The *C. elegans* genome contains two clusters of filamin-like sequences (WormBase WS205) (Harris et al., 2010). One set of predicted open reading frames (ORFs) is on chromosome IV (Y66H1B.2, Y66H1B.5, and Y66H1B.3) and the other is on chromosome X (C23F12.1 and C23F12.2). RNAi knockdown of Y66H1B.2, Y66H1B.5, and Y66H1B.3 resulted in striking defects including a dramatically reduced brood size (described below). Given this strong and reproducible phenotype, we chose to focus on the Y66H1B.2, Y66H1B.5, and Y66H1B.3 filamin cluster for further analysis.

Extensive cDNA sequencing of transcripts that span Y66H1B.3, Y66H1B.5, and Y66H1B.2 suggests these ORFs represent a single gene, which we have named *fln-1* (FiLamiN) (WormBase WS213) (Figure 1A). The full-length transcript includes all three computationally predicted ORFs and encodes a full-length *C. elegans* filamin ortholog (*fln-1a*) (Figure 1A). In addition to the full-length transcript, we detected two shorter transcripts (*fln-1b* and *c*) (Figure 1A). Y66H1B.3 and Y66H1B.2, but not Y66H1B.5, are trans-spliced to SL1 as determined by SL1 PCR and sequencing, which suggests the independent transcription of *fln-1a/b* and *fln-1c* (Figure 1A). The full-length filamin protein is predicted to be 2257 amino acids, while the C- and N-terminal truncations are predicted to be 1084 and 836 amino acids, respectively. The full-length filamin contains a well-conserved N-terminal ABD and 20 Ig-like repeats based on sequence alignments to human and the *Drosophila* filamin *cheerio*.

fln-1 is required for normal fertility

In order to genetically analyze the function of *fln-1*, we obtained two *fln-1* deletion alleles, *tm545* and *ok2611* from the Japanese National Bioresource Project and the *C. elegans* Gene Knockout Consortium, respectively. The *tm545* allele is a 263/17 bp deletion/insertion in the third exon of *fln-1a*, which causes a frameshift and a premature stop codon. The truncated protein is predicted to be 102 amino acids (Figure 1A). The *ok2611* allele is an in-frame 1763 bp deletion at the 3′ end of *fln-1a*, and is predicted to remove 455 amino acids (Figure 1A). The most striking defect of *tm545* hermaphrodites is a dramatic reduction in brood size (23 ± 7.9, n=26) compared to wildtype animals (298 ± 28.8, n=11) (Figure 2A). This phenotype is 100% penetrant in *fln-1(tm545)* animals. In contrast, *ok2611* animals are superficially wildtype and do not exhibit a brood size defect (290.8 ± 22.6, n=9) (Figure 2A). The brood sizes of heterozygous *tm545/+* animals (272.6 ± 38.5, n=9) and *tm545/ok2611* trans-heterozygotes (285.6 ± 15.9, n=7) are not significantly different from wildtype (Figure 2A). These results strongly suggest that the region removed by *ok2611* is not required for the function of filamin in fertility.

To confirm that the brood size defect of *fln-1(tm545)* is caused by disruption of *fln-1* function, we constructed transgenic nematodes carrying *fln-1* genomic DNA on an extrachromosomal array (*xbEx0827*). *fln-1(tm545)* animals carrying the full-length *fln-1* genomic region (Figure 1B) produce an average brood size of 195.1 ± 37.4 progeny (n=10) (Figure 2A). This robust rescue indicates the brood size defect in *tm545* animals is attributable to the deletion in *fln-1*. To investigate whether full-length *fln-1* is required for rescue of the brood size defect we attempted to rescue *fln-1(tm545)* with a genomic

fragment encompassing only Y66H1B.3 and Y66H1B.5 (*xbEx0817*). The *fln-1(tm545)* animals expressing this construct are not significantly different from non-transgenic siblings, with an average brood size of 18.8 ± 9.1 (n=18) progeny (Figure 2A). RNAi-mediated knockdown of *fln-1* with three independent RNAi constructs targeting Y66H1B.3, Y66H1B.5, or Y66H1B.2 (Figure 1A) phenocopies the *tm545* allele, reducing the brood size to 14.8 ± 5.2 (n=12), 15.6 ± 5 (n=14), and 15.5 ± 4.5 (n=10) progeny respectively (Figure 2B). These results indicate *fln-1(tm545)* is a strong hypomorphic allele, and suggest expression of full-length filamin is required for normal brood size.

Brood size defects are generally the result of somatic gonad, germ line, or embryogenesis defects. To investigate whether *fln-1* is required zygotically we mated *fln-1(tm545)* hermaphrodites to wildtype males. The brood size of *fln-1(tm545)* hermaphrodites mated to wildtype males (28.6 ± 6.2, n=7) is not significantly different from unmated hermaphrodites (23 ± 7.9, n=26; Student's t-test, p=0.09), indicating paternally supplied *fln-1* is not sufficient to restore normal brood size. To determine if depletion of filamin in the germline can account for the observed brood size defect we used the *rrf-1(pk1417)* mutant strain, which is defective for somatic RNAi, but has an apparently normal germline RNAi response (Sijen et al., 2001). The *rrf-1(pk1417)* animals have been used previously to demonstrate a somatic role for *fos-1* in the spermatheca (Hiatt et al., 2009). We found that *rrf-1(pk1417)* mutants treated with *fln-1* RNAi did not show a significantly different brood size (270.3 ± 45.1, n=8) from control RNAi treated *rrf-1(pk1417)* animals (307.2 ± 28.1, n=6; Student's t-test, p=0.1). Although this data does not entirely rule out a role for FLN-1 in the germ line, it does suggest that depletion of *fln-1* in the germ line does not contribute substantially to the observed brood size defects.

Wildtype animals produce embryos of consistent size and shape (Figure 2C). In contrast, most embryos laid by *fln-1(tm545)* hermaphrodites are misshapen (Figure 2D–F). Interestingly, some of the abnormally shaped embryos hatch (Figure 2E), while others fail at variable points during embryogenesis (Figure 2F). To characterize the embryo shape and possible embryogenesis defects we synchronized wildtype and *fln-1(tm545)* animals and examined embryo shape and hatching at 60, 70, 80, and 90 hours following L1 diapause recovery (Figure 2G). Throughout the time course, wildtype animals produce normally shaped and viable embryos (100%, n=561). The 60-hour time-point is shortly before the onset of egg laying and corresponds to the initial ovulations. At 60 hours *fln-1(tm545)* animals produce 67% normal embryos, 30% abnormally shaped but viable embryos, and 3% abnormally shaped embryos that fail to hatch. The proportion of abnormally shaped embryos and arrested abnormal embryos increases with maternal age. By 90 hours, 97% of the embryos are abnormally shaped, and 51% of these fail to hatch. Importantly, none of the normally shaped embryos arrest in *fln-1(tm545)* animals. These results strongly suggest that misshapen embryos and embryonic lethality are the result of a maternal defect during ovulation that results in physical damage to the embryos, rather than a defect during embryonic development.

fln-1 is expressed in the somatic gonad

To investigate the expression pattern of *fln-1* we created transgenic nematodes expressing GFP under the control of the *fln-1* promoter. GFP expression begins in early L4 stage and continues through adulthood in the uterus, spermatheca, and proximal gonadal sheath (Figure 3A–C). In addition to the somatic gonad, weak and variable GFP expression is evident in the posterior intestinal cells, anal depressor muscle, unidentified neurons, and the pharynx (data not shown). Due to silencing of repetitive extrachromosomal arrays in the germline, we cannot exclude the possibility that *fln-1* is also expressed in the germline. To determine the subcellular localization of FLN-1 we created transgenic nematodes carrying full-length FLN-1A fused to GFP at the N-terminus under the control of the native promoter

and 3′ UTR. GFP::FLN-1A localizes to punctate filaments in the spermathecal and uterine cells, and partially co-localizes with F-actin (Figure 3D–F and 3G–I, respectively). Importantly, the GFP::FLN-1A fusion protein (*xbEx1002*) rescues the brood size defect of *fln-1(tm545)* (99 ± 41.3, n=37) (Figure 2A), suggesting that the fusion protein is functional and represents normal FLN-1A subcellular localization. Incomplete rescue is likely due to overexpression of the transgene from the extrachromosomal arrays and mosaicism.

A primary function of filamin in other systems is to link the actin cytoskeleton to transmembrane receptors, such as integrins (Critchley, 2000). We hypothesized that filamin may be required to anchor the F-actin to integrins in the spermatheca. Filamin has been shown to interact with β-integrin cytoplasmic tails *in vitro*, and localizes to F-actin and focal adhesions in cultured cells (Kiema et al., 2006). To determine whether filamin and integrin co-localize in *C. elegans* we used the GFP::FLN-1A fusion and the β-integrin monoclonal antibody MH25 (Figure S1). Wildtype dissected gonads stained strongly for integrins in the sheath cells (Figure S1A–C) where they are organized into large dense bodies (Figure S1A) (Hall et al., 1999; Ono et al., 2007); however, the integrin staining in the spermatheca was much weaker and very diffuse (Figure S1D–F). We observed a similar staining pattern for talin (not shown). To our knowledge, dense bodies have not been described in the spermatheca. In contrast, GFP::FLN-1A is expressed strongly in the spermatheca and appears to localize in a punctate filament pattern (Figure S1D). Given the weak and diffuse staining of PAT-3 in the spermatheca we cannot conclude that filamin co-localizes with integrin in the spermatheca (Figure S1F).

fln-1 is required for normal exit of embryos from the spermatheca

We hypothesized that the reduced fertility and abnormal embryonic morphology in *fln-1(tm545)* animals might be the result of abnormal exit of embryos from the spermatheca. In wildtype animals, oocytes are ovulated into the spermatheca, fertilized, and then released into the uterus via the spermatheca-uterine valve (Figure 4A). The entire ovulation and fertilization process in wildtype animals is completed in less than ten minutes (Figure 4F, Movie 1A) (McCarter et al., 1999). In contrast, *fln-1(tm545)* animals showed a fully penetrant (n=29) spermathecal exit defect due to failure of the sp-ut valve to dilate (Figure 4G, Movie 1B). Our ovulation recordings of *fln-1(tm545)* animals do not show any overt abnormalities during the entry process. Importantly, the exit defect is rescued by the *fln-1(+)* and the GFP::FLN-1A transgenes (Movie 2A and B, respectively).

Due to the exit defect, multiple embryos accumulate in the spermatheca, which causes subsequent ovulations to fail. Embryos remain trapped in the spermatheca for at least six hours, the duration of the longest experiment. The initial three to four ovulations are normal in terms of entry, fertilization, and embryo development. Subsequent oocytes fail to enter the spermatheca due to accumulated embryos and are often fragmented by sheath cell contractions. In unanesthetized animals the spermatheca-uterine valve appears to prolapse between the second and third ovulations, presumably due to backpressure of oocytes and embryos, possibly aided by cycles of body-wall muscle contraction and relaxation. In order to assess the degree of trapping in unanesthetized animals, wildtype and *fln-1(tm545)* animals expressing spermatheca-specific *fkh-6::gfp* (Chang et al., 2004) were monitored while freely moving on plates. In *fln-1(tm545)* animals the spermatheca remains obviously distended and occupied by multiple embryos and oocytes (100%, n=160). Although wildtype animals also have distended spermatheca during ovulation, the spermatheca returns to normal size following oocyte exit. The short duration of ovulation results in only a small percentage of the wildtype population with distended spermathecae (5%, n=120). As previously discussed, the majority of the *fln-1(tm545)* brood is generated during the first several ovulation cycles, with some abnormally shaped, but surviving embryos generated afterward (Figure 2D–G). Following valve prolapse, *fln-1(tm545)* lay many unfertilized

oocytes suggesting inefficient fertilization. The misshapen embryos often result from pinched-off oocyte cytoplasm, but inappropriate sheath cell contractions and compaction in the spermatheca also contribute.

fln-1 is not required for spermathecal development

Given the reduced fertility of *fln-1(tm545)* animals and the prominent expression of *fln-1::gfp* in the proximal gonad, we speculated filamin may be required for proper development of these tissues. To assess development of the proximal gonad in *fln-1(tm545)* animals, we examined young-adult animals prior to the first ovulation using DIC microscopy. The spermatheca consists of three distinct regions, a distal neck-like constriction, a large central bag, and the spermatheca-uterine (sp-ut) valve (McCarter et al., 1997). The sp-ut valve is consists of a syncytial toroidal cell (sujn) and a core syncytial cell (sujc) (Kimble and Hirsh, 1979). The core cell is displaced during the first ovulation, and its fate is unknown.

Prior to the first ovulation, the morphology of the distal and central spermatheca is indistinguishable between wildtype and *fln-1(tm545)* animals by DIC (Figure 4B, C). In addition, the apical junctions between spermathecal cells were visualized with *jam-1::gfp* and the anti-JAM-1 monoclonal antibody (MH27) (Koppen et al., 2001). Junctions were indistinguishable from wildtype in *fln-1(tm545)* and *fln-1* RNAi animals (data not shown). We also used *fkh-6::gfp* (Chang et al., 2004; Gissendanner et al., 2008), a spermatheca developmental marker, to assess morphogenesis of the spermatheca. In wildtype animals *fkh-6::gfp* is expressed in the distal and central spermatheca, but not in the sp-ut. An identical staining pattern is observed in *fln-1(tm545)* animals (Figure 4B, C). In older adult wildtype animals the spermatheca appears as a compact structure (Figure 4D). In contrast, the *fln-1(tm545)* spermatheca is distended due to accumulated embryos (Figure 4E). The spermatheca remains distended and occupied by embryos and fragmented oocytes for the duration of adulthood. Importantly, the spermatheca does not disintegrate at any point. .

fln-1 is required for correct morphology of the spermatheca-uterine valve

We also examined the spermatheca-uterine (sp-ut) valve using DIC microscopy in wildtype and *fln-1(tm545)* animals (Figure 5A, B). In wildtype animals the sp-ut is a toroid produced by the donut-shaped sujn cell, with a rod-like opening in the center formed by the sujn and sujc cells (Figure 5A) (Kimble and Hirsh, 1979). In contrast, the sp-ut valve of *fln-1(tm545)* animals appeared creased or folded and lacked the characteristic wildtype morphology, suggesting that filamin is required to maintain the proper morphology of the sujn cell (Figure 5B). To visualize the morphology of the sujn cell in *fln-1(tm545)* animals we used *tag-312::gfp*, which is expressed in the sujn and the uterus. We thought the crumpled appearance of the sujn cell might indicate a closed valve, through which oocytes might not be able to exit. To visualize the inside of the valve, we used a *cog-1::gfp* (Palmer et al., 2002) fusion to label the sujc cell, which projects filopodia from the uterus into the spermatheca through the sp-ut valve (Figure 5C, D). The expression pattern of *cog-1::gfp* was essentially identical in wildtype and *fln-1(tm545)* animals, suggesting that the valve does form a channel connecting the spermatheca and the uterus (Figure 5E, F). In addition, we regularly observe sperm passing from the spermatheca into the uterus of *fln-1(tm545)* animals during ovulation. In motile animals, embryos do eventually exit the spermatheca through the valve into the uterus, and do not break out through the spermathecal wall.

Even though the valve appears to be open and of apparently normal diameter in *fln-1(tm545)* animals, the crumpled morphology of the apical surface of the sujn cells suggests that the valve might not be functional. A non-functional valve could account for the trapped oocyte phenotype seen in the filamin mutants. Alternatively, *fln-1* function may be required in the

spermatheca itself as well as in the valve for proper exit of fertilized oocytes. We used the GFP::FLN-1A transgene in the *fln-1(tm545)* background to determine which spermathecal cells require FLN-1 for normal ovulation. Animals which visibly expressed GFP::FLN-1A only in the sp-ut valve had a morphologically normal valve, but contained trapped embryos (100%; n=8). In contrast, animals expressing GFP::FLN-1A in the spermatheca and the sp-ut valve were essentially wildtype and contained no trapped embryos (90%; n=29). Therefore, expression of GFP::FLN-1A in the sp-ut valve apparently restores normal morphology of the valve, but is not sufficient to rescue the exit defect. These results are consistent with the hypothesis that filamin is required to maintain the structure of the valve, but is also necessary in the spermatheca. These results suggest that filamin is required to maintain the structure of the sp-ut valve, but may also be required in the spermatheca itself to transduce signals in addition to playing a structural role.

F-actin is disorganized in the spermatheca and uterus of *fln-1(tm545)* mutants

The most well characterized role of filamins is organization of the actin cytoskeleton (Stossel et al., 2001). The actin cytoskeleton is essential for proper ovulation in *C. elegans*, and is required for the structure and function of the myoepithelial sheath cells, spermatheca, and uterus (McCarter et al., 1999; Ono et al., 2007). To visualize actin in the gonadal sheath, spermatheca, and uterus of wildtype and *fln-1(tm545)* animals, we stained dissected *C. elegans* gonads with Texas Red-X phalloidin. Sheath cell actin was indistinguishable from wildtype in *fln-1(tm545)* animals, with the expected longitudinally arranged actin filaments in the distal sheath cells and more circumferential filaments in the contractile proximal sheath cells (Figure 6A). In wildtype spermathecal cells, regularly spaced circumferential actin bundles can clearly be visualized (Figure 6B). In stark contrast, in adult *fln-1(tm545)* animals, spermathecal F-actin was bundled into thick, cortical bundles and localized to the cell-cell junctions (Figure 6D). In the uterus of wildtype animals, F-actin is organized predominantly longitudinally and originates at the spermatheca-uterine lariat (Figure 6C) (Strome, 1986). Interestingly, the spermatheca-uterine lariat is severely disorganized in filamin mutant animals and lacks the characteristic branching filaments (Figure 6E). *fln-1* is the first gene known to be required for maintenance of the spermatheca-uterine lariat, and may play a role in strengthening the uterus to withstand the pressure of accumulating embryos.

The first ovulation event coincides with a dramatic rearrangement of the spermathecal actin cytoskeleton. Pre-ovulation spermathecal actin is not organized into tight circumferential filaments (Figure 7A). After the first ovulation, these filaments are formed and persist through many cycles of fertilization (Figure 7B–E). This suggests that the adult spermathecal cytoskeleton is established shortly before or during the first ovulation. Spermathecal actin in *fln-1(tm545)* animals, before the first ovulation, resembles that of wildtype animals, but is not entirely normal (Figure 7F). Following the first ovulation of *fln-1(tm545)* animals the F-actin appears to reorganize as in wildtype animals, although the filaments are not as robust (Figure 7G). Young adult *fln-1(tm545)* spermathecae lack the cortical bundles characteristic of later stage animals (Figures 6D and 7J). Our F-actin staining at various ages suggests that spermathecal actin progressively degenerates following the first failed ovulation (Figure 7H–J). In addition, the early time points (55–65 hours) show a greater degree of variability than the later time points (72 hours). The variability is likely due to rapid changes that occur between the first and second ovulations. These results suggest that filamin is primarily required to maintain the F-actin cytoskeleton in response to stretching by the oocyte during ovulation. Our data do not rule out a role for filamin in the initial F-actin organization.

The phospholipase PLC-1 is also required for the exit of embryos from the spermatheca (Kariya et al., 2004). The *plc-1(rx1)* putative null animals phenocopy the exit defect of

fln-1(tm545) animals, and retain multiple embryos in the spermatheca. PLC-1 is broadly expressed, and has been shown to have a role in embryogenesis, in addition to its role during ovulation (Hiatt et al., 2009; Vazquez-Manrique et al., 2008). We hypothesized that, if stretching induced by accumulated embryos causes the actin to be redistributed to the cell boundaries, the actin cytoskeleton in *plc-1(rx1)* spermathecal cells might be similarly disrupted. Surprisingly, spermathecal and uterine F-actin in *plc-1(rx1)* animals was indistinguishable from wildtype, despite stress caused by the retained embryos (Figure 6F, G). F-actin staining of *fln-1(tm545); plc-1(rx1)* double mutant animals was indistinguishable from that of *fln-1(tm545)* single mutants (data not shown). Also, the sp-ut valve in *plc-1(rx1)* animals appears normal by DIC microscopy. These results suggest that PLC-1 may not play a significant role in the maintenance of the actin cytoskeleton or in sp-ut valve morphology, but instead PLC-1 may be required to produce a signal that allows exit of the fertilized embryo from the spermatheca. *fln-1(tm545); plc-1(rx1)* double mutant animals are viable and show a decreased brood size (16 ± 4, n=15), which is not significantly different from the *plc-1(rx1)* single mutant animals (12.4 ± 5.9, n=9; Student's t-test, p=0.1). These data suggest that *fln-1* and *plc-1* act in the same genetic pathway to allow exit of embryos from the spermatheca, perhaps through modulation of phosphoinositol signaling.

Discussion

Filamin is a large cytoskeletal protein that functions as a physical and signaling scaffold, and has been implicated in a wide variety of human disorders. We show that the *C. elegans* filamin ortholog FLN-1 is required to organize actin in the spermatheca and uterus, and to control the exit of embryos from the spermatheca. Filamin mutation or RNAi-mediated depletion of *fln-1* results in a highly penetrant spermathecal exit defect during ovulation. Filamin-deficient animals accumulate embryos in the spermatheca, and consequently exhibit dramatically reduced brood sizes. The ovulation exit defect manifests as abnormally shaped, variably arrested embryos, which may be a general characteristic of spermathecal exit mutants. The proportion of misshapen and inviable embryos rapidly increases after the first four to five ovulations, suggesting the disrupted exit process in *fln-1(tm545)* animals physically damages the embryos.

FLN-1 is not required for spermathecal or uterine development *per se*; however, filamin is required for normal spermatheca-uterine valve morphology. The wildtype sp-ut valve is a toroid formed by the fusion of the sujn cells, which appears as an ellipse with a dense core and smooth edges when viewed by DIC microscopy. The sp-ut valve in *fln-1(tm545)* animals lacks the characteristic wildtype morphology on the basal surface, and is more crumpled on the apical surface. Our analysis shows that the sujn and sujc cells are present, and that the valve connects the spermatheca to the uterus. In motile animals, embryos exit the spermatheca after the second or third ovulation weakening the sp-ut valve and causing valve prolapse. The spermatheca remains occupied by multiple embryos and oocytes following valve prolapse. Expression of GFP::FLN-1A only in the valve restores the normal morphology and prevents valve prolapse, but is not sufficient for normal exit. This is similar to the *plc-1* phenotype where the valve does not prolapse, but the embryos do not exit the spermatheca in a timely manner. These results suggest that a morphologically normal valve is not sufficient for exit of embryos from the spermatheca.

Filamin-deficient animals show F-actin disorganization in the spermatheca and uterus that worsens as embryos accumulate. This phenotype suggests that filamin is necessary to maintain the actin cytoskeleton under stress. Prior to the first ovulation, spermathecal F-actin is comparatively normal. PLC-1/Phospholipase C-ε mutant animals phenocopy the filamin exit defect and accumulate embryos; however, the F-actin appears unaffected. These results suggest that physical stress is not sufficient to cause F-actin disorganization and that

the effect is specific to loss of filamin. The cytoskeleton is necessary for many aspects of cell behavior, such as trafficking and signaling, making it difficult to differentiate between direct and indirect effects of F-actin disorganization. Perturbation of the actin cytoskeleton by loss of filamin may have diverse downstream effects. Based on progression of the F-actin degeneration in the spermatheca it seems unlikely that F-actin disorganization is the sole factor responsible for the exit defect. All first ovulation embryos are trapped in the spermatheca despite relatively normal F-actin organization. Although our attempts to image F-actin in the sp-ut valve have been unsuccessful due to the size of the valve, we know that rescuing the valve morphology, and presumably any F-actin defects, is not sufficient for normal exit. Our data, and the previous *plc-1* data, show that normal structure is not sufficient for the exit process, and suggest that an underlying signaling pathway plays an important role.

In filamin mutant animals filamentous actin is mislocalized to cell-cell junctions, which suggests the cytoskeleton may not be properly anchored throughout the cell. Our analysis of the GFP::FLN-1A fusion protein shows FLN-1 partially co-localizes to F-actin in the spermatheca and the uterus in a punctate filamentous pattern. Surprisingly, our β-integrin immunostaining shows diffuse staining in the spermatheca and a lack of clear dense bodies, despite strong staining of the sheath cells. Given the weak and diffuse integrin staining in the spermatheca we cannot conclude that integrin and filamin co-localize. The possibility that FLN-1 may not need to associate with integrin to promote proper spermathecal function is also suggested by the *fln-1(ok2611)* allele, which removes the integrin-association repeat of FLN-1 but does not affect ovulation. The pattern of dense body staining in the sheath and the spermatheca is consistent with the different functions of the two tissues. The sheath contracts rapidly and strongly, while the spermatheca shows no such contractions. Integrin-based adhesions in the spermatheca are likely required for development of the spermatheca, but they may not be required for the function of the adult spermatheca (Ono et al., 2007).

The entry process is regulated by EGF signaling from the oocyte to the sheath cells and the distal spermatheca. Upon activation of LET-23/EGFR, PLC-3/PLC-γ is probably activated by LET-23 (Clandinin et al., 1998; Yin et al., 2004). In contrast, the potentiating signal for sp-ut dilation and embryo release from the spermatheca into the uterus is unknown. Upon entry of the oocyte into the spermatheca, the spermathecal cells become stretched. We predict this stretching could result in conformational changes to the filamin dimer and revelation of cryptic binding sites. Alternatively, filamin may have a role in cell response to stretch not directly sensed by the filamin molecule, such as activation of stretch-gated ion channels (Orr et al., 2006). For example, filamin interacts with flow-sensitive polycystin ion channels in epithelial and endothelial cells (Sharif-Naeini et al., 2009), suggesting that in addition to being a direct mechanosensor, filamin may modulate the cytoskeleton to sensitize or desensitize cells to physical force.

Our working model is that entry of the oocyte into the spermatheca triggers a series of events involving FLN-1 and PLC-1 that leads to relaxation of the sp-ut valve and exit of the embryo into the uterus. Based on our time-lapse recordings of ovulation, the spermatheca and the sp-ut valve do not appear to actively contract or dilate, but appear to gradually relax as the oocyte moves forward. The gradual relaxation of the spermatheca and the sp-ut is in sharp contrast to the forceful and swift gonadal sheath contractions, suggesting a different mechanism. Consistent with the idea that IP_3 signaling controls sp-ut dilation, depletion of IP_3 by LFE-2 over-expression under the heatshock promoter (Clandinin et al., 1998) or PLC-1 loss-of-function causes an exit defect (Kariya et al., 2004). We therefore hypothesize that filamin-depleted animals are also unable to produce or respond to IP_3 signals, resulting in the exit defect. In support of this idea, filamin has been shown to interact with

phosphoinositol signaling pathways in cell culture, usually as a downstream effector (Bourguignon et al., 2006; Dyson et al., 2001; Takabayashi et al.).

Taken together, our results suggest that filamin is required to maintain circumferential actin bundles in the spermatheca under stress and to act as a stretch-sensitive signaling scaffold. Filamin may potentiate or transduce the phosphoinositol and calcium signals that result in the sp-ut valve dilation and exit of oocytes from the spermatheca. This work provides evidence that FLN-1/filamin plays a structural and signaling role in the *C. elegans* somatic gonad. Our results directly demonstrate the importance of filamin in tissues undergoing stress *in vivo*. Studies are underway to more precisely determine the position of FLN-1 in the phosphoinositol signaling pathway, and to identify additional genes that are required for the exit of oocytes from the spermatheca. Given the striking conservation of FLN-1 sequence, structure, and interaction partners from worm to human, elucidation of the function of filamin in *C. elegans* will continue to provide important insights into the fundamental regulation of mechanosensation and tissue function.

Materials and Methods

C. elegans strains and culture

All nematode strains were cultured on NGM agar plates with OP50 *E. coli* at 20°C. Nematode observations and manipulations were performed at 20°C unless otherwise noted. The *C. elegans* filamin allele *fln-1(tm545)* was obtained from the Japanese National Bioresource Project and outcrossed three times to wildtype animals to create the strain UN0810 *fln-1(tm545)*. All other strains were obtained from the Caenorhabditis Genetics Center, with the exception of PS4195, which was kindly provided by Paul Sternberg. For a list of strains used in this study, please see Table S1.

Genetic crosses

fln-1(*ok2611*)/*fln-1(tm545)* trans-heterozygous animals were generated by crossing *fln-1(tm545)* males to *fln-1*(*ok2611*) hermaphrodites. F1 animals of the putative genotype *tm545*/*ok2611* were segregated for brood size assays. The first ten F2 progeny were genotyped using PCR to confirm the presence of *tm545* and *ok2611* alleles.

Construction of the *fln-1(tm545); plc-1(rx1)* double mutant was performed by crossing *fln-1(tm545)* males to *plc-1(rx1)* hermaphrodites. F1 animals of the putative genotype *tm545*/+ were subcloned. F2 animals were subcloned and the genotype determined by PCR. Homozygosity of the alleles was confirmed by PCR genotyping of the progeny.

RNA interference

RNA interference was performed by feeding animals dsRNA-expressing HT115 DE3 *E. coli* essentially as described (Cram et al., 2006). Eggs were obtained from gravid hermaphrodites using alkaline hypochlorite solution and transferred to NGM/Carbenicillin/IPTG plates seeded with RNAi bacteria. RNAi experiments were performed at 20°C. RNAi targeting constructs for Y66H1B.3, Y66H1B.5, and Y66H1B.2 were constructed by PCR amplification of wildtype cDNA using engineered restriction sites, and subsequently cloned into pPD129.36 (Fire Vector Kit). Empty pPD129.36 vector was used as a negative control in RNAi experiments. All primer sequences and cloning details available upon request.

Brood size assays

Total number of hatchlings produced by a single animal was determined by segregating L4 parental animals to individual, freshly seeded plates and aspirating larvae each day, beginning two days after transfer and continuing for at least five days.

Embryo shape and embryonic lethality assay

Animal populations were synchronized by hatching embryos in the absence of food for 20 hours in M9 buffer. The arrested L1 animals were transferred to NGM plates seeded with OP50 *E. coli*. Worms were collected in M9, dissected, and mounted on 1.5% agarose pads at 60, 70, 80, and 90 hours after being placed on food. Embryo shapes were scored immediately using DIC microscopy, then allowed to hatch overnight at 20°C. The slides were examined again within 24 hours to determine which embryos hatched.

Time-lapse microscopy

Animals were anesthetized with 0.01% tetramisole and 0.1% tricaine in M9 buffer (Kirby et al., 1990; McCarter et al., 1997), mounted on 1.5% agarose pads and imaged using a 60x oil-immersion objective with a Nikon Eclipse 80i microscope equipped with a SPOT RT3 CCD camera (Diagnostic Instruments; Sterling Heights, MI, USA). Images were captured at a rate of 0.5 frames per second (FPS) using SPOT Advanced version 4.6.4.6 (Diagnostic Instruments; Sterling Heights, MI, USA) software. The individual frames (TIFF with JPEG compression) were resized to 400 × 300 pixels and assembled into time-lapse movies using SPOT Advanced software at 10 FPS. The Audio Video Interleave (AVI) files generated by SPOT Advanced were imported into QuickTime Pro version 7.6.2 (Apple; Cupertino, CA, USA) and compressed using H.264, then exported as Moving Picture Experts Group, Standard 4 (MPEG-4) movies. The time-lapse movies are 20-fold faster than real-time.

Construction of *fln-1::gfp* transgenic animals

GoTaq Green MasterMix (Promega; Madison, WI, USA) was used to amplify a 957 bp region 5′ to Y66H1B.3 flanked by engineered restriction sites HindIII and BamHI. The HindIII-BamHI fragment was cloned into pPD95.77 (Fire Vector Kit) to create pUN70. The plasmid was isolated from *E. coli* and directly used in microinjection at an approximate concentration of 100 μg/mL. Transgenic strains were created by standard germline transformation technique (Mello et al., 1991) of wildtype animals to create strain UN0811 *xbEx0811[fln-1::gfp]*.

Construction of GFP::FLN-1A transgenic animals

Full-length *fln-1a* transcript was amplified by PCR from wildtype cDNA using Phusion DNA Polymerase (New England Biolabs; Ipswich, MA, USA). The amplicon was then inserted into pUN88 between the *fln-1* promoter and 3′ UTR to create pUN97 using the In-Fusion enzyme (Clontech; Mountain View, CA, USA). pUN97 was purified and mixed with co-injection marker *rol-6(su1006)* (pRF4) to a final concentration of approximately 50 μg/mL. The DNA mixture was injected into wildtype animals to establish the extrachromosomal array *xbEx1002[fln-1::gfp::fln-1a, rol-6(su1006)]*. The rescuing construct was introduced into the *fln-1(tm545)* background by genetic cross to create strain UN1003.

fln-1 genomic rescue

LongAmp (New England Biolabs, Ipswich, MA, USA) was used to amplify the 19 kb genomic region encompassing ORFs Y66H1B.3, Y66H1B.5, and Y66H1B.2, including 1.5 kb of 5′ and 3′ flanking sequences. Transgenic animals were created by standard microinjection germline transformation. The long-range amplicon was agarose gel-purified and mixed with co-injection marker *sur-5::gfp* (pTG96) and water to a final concentration of 100 μg/mL. The DNA mixture was injected into wildtype animals to establish the extrachromosomal array *xbEx0827[fln-1(+), sur-5::gfp]*. The rescuing construct was introduced into the *fln-1(tm545)* background by genetic cross to create strain UN0903. The same process was used to construct an extrachromosomal array with a truncated *fln-1*

genomic region encompassing Y66H1B.3 and Y66H1B.5, *xbEx0917[fln-1(Y66H1B.3/5), sur-5::gfp]*.

Construction of sujn-specific marker

To construct an sujn-specific GFP marker we used WormBase expression data to identify candidate genes expressed in the sujn cell. We used Phusion DNA Polymerase to amplify the putative *tag-312* promoter (1 kb upstream) and cloned it into pPD95_77. The plasmid was isolated from *E. coli* and mixed with co-injection marker *rol-6(su1006)* (pRF4) to a final concentration of approximately 50 μg/mL. Transgenic strains were created by standard germline transformation technique (Mello et al., 1991) of wildtype animals to create strain UN1019 *xbEx1019[tag-312::gfp, rol-6(su1006)]*. The transgene was introduced into *fln-1(tm545)* background by genetic cross.

Immunofluorescence

F-actin and PAT-3 immunoflourescence was performed as described (Ono et al., 2007). Briefly, partially synchronized populations were dissected using a 25-gauge hypodermic needle in PBS, and dissected gonads were fixed in 3.7% formaldehyde in PBS for 20 minutes at room temperature. For F-actin staining, following the formaldehyde fixation the animals were washed twice with PBST (PBS + 0.1% Triton X-100) for 20 minutes, and then incubated with 0.4 U/mL of Texas Red-X phalloidin in PBS (Invitrogen, Carlsbad, CA, USA) overnight at 4°C or 4 hours at room temperature, washed with PBS, and mounted on 1.5% agarose pads for observation. For PAT-3 staining, fixed animals were incubated with MH25 anti-PAT-3 antibodies (1:100 dilution) overnight at 4°C, followed by Cy3-conjugated donkey anti-mouse (Jackson ImmunoResearch Laboratories; West Grove, PA, USA) for 4 hours at room temperature, washed twice with PBS, and mounted on 1.5% agarose pads for observation. Fluorescence microscopy was performed on a Nikon Eclipse 80i microscope equipped for epifluorescence. Images were captured with a SPOT RT3 CCD camera using SPOT Advanced software (Diagnostic Instruments; Sterling Heights, MI, USA). This fixation procedure preserves GFP fluorescence.

Supplementary Material

Refer to Web version on PubMed Central for supplementary material.

Acknowledgments

Many *C. elegans* strains were provided by the Caenorhabditis Genetic Center, which is funded by the National Center for Research Resources, National Institutes of Health. We thank Paul Sternberg for providing multiple strains, and Anne Hart for helpful discussions. We thank Jose Orozco for help with experiments. I.K. and E.J.C. are partially supported by Northeastern University and a grant from NIH.

References

Annesley SJ, Bandala-Sanchez E, Ahmed AU, Fisher PR. Filamin repeat segments required for photosensory signalling in Dictyostelium discoideum. BMC Cell Biol. 2007; 8:48. [PubMed: 17997829]

Bourguignon LY, Gilad E, Brightman A, Diedrich F, Singleton P. Hyaluronan-CD44 interaction with leukemia-associated RhoGEF and epidermal growth factor receptor promotes Rho/Ras co-activation, phospholipase C epsilon-Ca2+ signaling, and cytoskeleton modification in head and neck squamous cell carcinoma cells. J Biol Chem. 2006; 281:14026–14040. [PubMed: 16565089]

Bui YK, Sternberg PW. Caenorhabditis elegans inositol 5-phosphatase homolog negatively regulates inositol 1,4,5-triphosphate signaling in ovulation. Mol Biol Cell. 2002; 13:1641–1651. [PubMed: 12006659]

Calderwood DA, Huttenlocher A, Kiosses WB, Rose DM, Woodside DG, Schwartz MA, Ginsberg MH. Increased filamin binding to beta-integrin cytoplasmic domains inhibits cell migration. Nat Cell Biol. 2001; 3:1060–1068. [PubMed: 11781567]

Chang W, Tilmann C, Thoemke K, Markussen FH, Mathies LD, Kimble J, Zarkower D. A forkhead protein controls sexual identity of the C. elegans male somatic gonad. Development. 2004; 131:1425–1436. [PubMed: 14993191]

Clandinin TR, DeModena JA, Sternberg PW. Inositol trisphosphate mediates a RAS-independent response to LET-23 receptor tyrosine kinase activation in C. elegans. Cell. 1998; 92:523–533. [PubMed: 9491893]

Cram EJ, Shang H, Schwarzbauer JE. A systematic RNA interference screen reveals a cell migration gene network in C. elegans. J Cell Sci. 2006; 119:4811–4818. [PubMed: 17090602]

Critchley DR. Focal adhesions - the cytoskeletal connection. Curr Opin Cell Biol. 2000; 12:133–139. [PubMed: 10679361]

Dyson JM, O'Malley CJ, Becanovic J, Munday AD, Berndt MC, Coghill ID, Nandurkar HH, Ooms LM, Mitchell CA. The SH2-containing inositol polyphosphate 5-phosphatase, SHIP-2, binds filamin and regulates submembraneous actin. J Cell Biol. 2001; 155:1065–1079. [PubMed: 11739414]

Feng Y, Walsh CA. The many faces of filamin: a versatile molecular scaffold for cell motility and signalling. Nat Cell Biol. 2004; 6:1034–1038. [PubMed: 15516996]

Ferrer I, Olive M. Molecular pathology of myofibrillar myopathies. Expert Rev Mol Med. 2008; 10:e25. [PubMed: 18764962]

Fox JW, Lamperti ED, Eksioglu YZ, Hong SE, Feng Y, Graham DA, Scheffer IE, Dobyns WB, Hirsch BA, Radtke RA, Berkovic SF, Huttenlocher PR, Walsh CA. Mutations in filamin 1 prevent migration of cerebral cortical neurons in human periventricular heterotopia. Neuron. 1998; 21:1315–1325. [PubMed: 9883725]

Gehler S, Baldassarre M, Lad Y, Leight JL, Wozniak MA, Riching KM, Eliceiri KW, Weaver VM, Calderwood DA, Keely PJ. Filamin A-beta1 integrin complex tunes epithelial cell response to matrix tension. Mol Biol Cell. 2009; 20:3224–3238. [PubMed: 19458194]

Gissendanner CR, Kelley K, Nguyen TQ, Hoener MC, Sluder AE, Maina CV. The Caenorhabditis elegans NR4A nuclear receptor is required for spermatheca morphogenesis. Dev Biol. 2008; 313:767–786. [PubMed: 18096150]

Gorlin JB, Yamin R, Egan S, Stewart M, Stossel TP, Kwiatkowski DJ, Hartwig JH. Human endothelial actin-binding protein (ABP-280, nonmuscle filamin): a molecular leaf spring. J Cell Biol. 1990; 111:1089–1105. [PubMed: 2391361]

Hall DH, Winfrey VP, Blaeuer G, Hoffman LH, Furuta T, Rose KL, Hobert O, Greenstein D. Ultrastructural features of the adult hermaphrodite gonad of Caenorhabditis elegans: relations between the germ line and soma. Dev Biol. 1999; 212:101–123. [PubMed: 10419689]

Harris TW, Antoshechkin I, Bieri T, Blasiar D, Chan J, Chen WJ, De La Cruz N, Davis P, Duesbury M, Fang R, Fernandes J, Han M, Kishore R, Lee R, Muller HM, Nakamura C, Ozersky P, Petcherski A, Rangarajan A, Rogers A, Schindelman G, Schwarz EM, Tuli MA, Van Auken K, Wang D, Wang X, Williams G, Yook K, Durbin R, Stein LD, Spieth J, Sternberg PW. WormBase: a comprehensive resource for nematode research. Nucleic Acids Res. 2010; 38:D463–467. [PubMed: 19910365]

Hart AW, Morgan JE, Schneider J, West K, McKie L, Bhattacharya S, Jackson IJ, Cross SH. Cardiac malformations and midline skeletal defects in mice lacking filamin A. Hum Mol Genet. 2006; 15:2457–2467. [PubMed: 16825286]

Hiatt SM, Duren HM, Shyu YJ, Ellis RE, Hisamoto N, Matsumoto K, Kariya K, Kerppola TK, Hu CD. Caenorhabditis elegans FOS-1 and JUN-1 regulate plc-1 expression in the spermatheca to control ovulation. Mol Biol Cell. 2009; 20:3888–3895. [PubMed: 19570917]

Himmel M, Van Der Ven PF, Stocklein W, Furst DO. The limits of promiscuity: isoform-specific dimerization of filamins. Biochemistry. 2003; 42:430–439. [PubMed: 12525170]

Hubbard EJ, Greenstein D. The Caenorhabditis elegans gonad: a test tube for cell and developmental biology. Dev Dyn. 2000; 218:2–22. [PubMed: 10822256]

Kainulainen T, Pender A, D'Addario M, Feng Y, Lekic P, McCulloch CA. Cell death and mechanoprotection by filamin a in connective tissues after challenge by applied tensile forces. J Biol Chem. 2002; 277:21998–22009. [PubMed: 11909861]

Kariya K, Bui YK, Gao X, Sternberg PW, Kataoka T. Phospholipase Cepsilon regulates ovulation in Caenorhabditis elegans. Dev Biol. 2004; 274:201–210. [PubMed: 15355798]

Kiema T, Lad Y, Jiang P, Oxley CL, Baldassarre M, Wegener KL, Campbell ID, Ylanne J, Calderwood DA. The molecular basis of filamin binding to integrins and competition with talin. Mol Cell. 2006; 21:337–347. [PubMed: 16455489]

Kimble J, Hirsh D. The postembryonic cell lineages of the hermaphrodite and male gonads in Caenorhabditis elegans. Dev Biol. 1979; 70:396–417. [PubMed: 478167]

Kirby C, Kusch M, Kemphues K. Mutations in the par genes of Caenorhabditis elegans affect cytoplasmic reorganization during the first cell cycle. Dev Biol. 1990; 142:203–215. [PubMed: 2227096]

Koppen M, Simske JS, Sims PA, Firestein BL, Hall DH, Radice AD, Rongo C, Hardin JD. Cooperative regulation of AJM-1 controls junctional integrity in Caenorhabditis elegans epithelia. Nat Cell Biol. 2001; 3:983–991. [PubMed: 11715019]

Li MG, Serr M, Edwards K, Ludmann S, Yamamoto D, Tilney LG, Field CM, Hays TS. Filamin is required for ring canal assembly and actin organization during Drosophila oogenesis. J Cell Biol. 1999; 146:1061–1074. [PubMed: 10477759]

McCarter J, Bartlett B, Dang T, Schedl T. Soma-germ cell interactions in Caenorhabditis elegans: multiple events of hermaphrodite germline development require the somatic sheath and spermathecal lineages. Dev Biol. 1997; 181:121–143. [PubMed: 9013925]

McCarter J, Bartlett B, Dang T, Schedl T. On the control of oocyte meiotic maturation and ovulation in Caenorhabditis elegans. Dev Biol. 1999; 205:111–128. [PubMed: 9882501]

Mello CC, Kramer JM, Stinchcomb D, Ambros V. Efficient gene transfer in C.elegans: extrachromosomal maintenance and integration of transforming sequences. EMBO J. 1991; 10:3959–3970. [PubMed: 1935914]

Miller MA, Nguyen VQ, Lee MH, Kosinski M, Schedl T, Caprioli RM, Greenstein D. A sperm cytoskeletal protein that signals oocyte meiotic maturation and ovulation. Science. 2001; 291:2144–2147. [PubMed: 11251118]

Nakamura F, Osborn TM, Hartemink CA, Hartwig JH, Stossel TP. Structural basis of filamin A functions. J Cell Biol. 2007; 179:1011–1025. [PubMed: 18056414]

Ono K, Yu R, Ono S. Structural components of the nonstriated contractile apparatuses in the Caenorhabditis elegans gonadal myoepithelial sheath and their essential roles for ovulation. Dev Dyn. 2007; 236:1093–1105. [PubMed: 17326220]

Orr AW, Helmke BP, Blackman BR, Schwartz MA. Mechanisms of mechanotransduction. Dev Cell. 2006; 10:11–20. [PubMed: 16399074]

Palmer RE, Inoue T, Sherwood DR, Jiang LI, Sternberg PW. Caenorhabditis elegans cog-1 locus encodes GTX/Nkx6.1 homeodomain proteins and regulates multiple aspects of reproductive system development. Dev Biol. 2002; 252:202–213. [PubMed: 12482710]

Popowicz GM, Schleicher M, Noegel AA, Holak TA. Filamins: promiscuous organizers of the cytoskeleton. Trends Biochem Sci. 2006; 31:411–419. [PubMed: 16781869]

Sharif-Naeini R, Folgering JH, Bichet D, Duprat F, Lauritzen I, Arhatte M, Jodar M, Dedman A, Chatelain FC, Schulte U, Retailleau K, Loufrani L, Patel A, Sachs F, Delmas P, Peters DJ, Honore E. Polycystin-1 and -2 dosage regulates pressure sensing. Cell. 2009; 139:587–596. [PubMed: 19879844]

Shifrin Y, Arora PD, Ohta Y, Calderwood DA, McCulloch CA. The role of FilGAP-filamin A interactions in mechanoprotection. Mol Biol Cell. 2009; 20:1269–1279. [PubMed: 19144823]

Sijen T, Fleenor J, Simmer F, Thijssen KL, Parrish S, Timmons L, Plasterk RH, Fire A. On the role of RNA amplification in dsRNA-triggered gene silencing. Cell. 2001; 107:465–476. [PubMed: 11719187]

Sokol NS, Cooley L. Drosophila filamin is required for follicle cell motility during oogenesis. Dev Biol. 2003; 260:260–272. [PubMed: 12885568]

Stefanova M, Meinecke P, Gal A, Bolz H. A novel 9 bp deletion in the filamin a gene causes an otopalatodigital-spectrum disorder with a variable, intermediate phenotype. Am J Med Genet A. 2005; 132:386–390. [PubMed: 15654694]

Stossel TP, Condeelis J, Cooley L, Hartwig JH, Noegel A, Schleicher M, Shapiro SS. Filamins as integrators of cell mechanics and signalling. Nat Rev Mol Cell Biol. 2001; 2:138–145. [PubMed: 11252955]

Strome S. Fluorescence visualization of the distribution of microfilaments in gonads and early embryos of the nematode Caenorhabditis elegans. J Cell Biol. 1986; 103:2241–2252. [PubMed: 3782297]

Takabayashi T, Xie MJ, Takeuchi S, Kawasaki M, Yagi H, Okamoto M, Tariqur RM, Malik F, Kuroda K, Kubota C, Fujieda S, Nagano T, Sato M. LL5{beta} directs the translocation of Filamin A and SHIP2 to sites of PtdIns(3,4,5)P3 accumulation and PtdIns(3,4,5)P3 localization is mutually modified by co-recruited SHIP2. J Biol Chem. 2010

Vazquez-Manrique RP, Nagy AI, Legg JC, Bales OA, Ly S, Baylis HA. Phospholipase C-epsilon regulates epidermal morphogenesis in Caenorhabditis elegans. PLoS Genet. 2008; 4:e1000043. [PubMed: 18369461]

Yin X, Gower NJ, Baylis HA, Strange K. Inositol 1,4,5-trisphosphate signaling regulates rhythmic contractile activity of myoepithelial sheath cells in Caenorhabditis elegans. Mol Biol Cell. 2004; 15:3938–3949. [PubMed: 15194811]

Zhou X, Tian F, Sandzen J, Cao R, Flaberg E, Szekely L, Cao Y, Ohlsson C, Bergo MO, Boren J, Akyurek LM. Filamin B deficiency in mice results in skeletal malformations and impaired microvascular development. Proc Natl Acad Sci U S A. 2007; 104:3919–3924. [PubMed: 17360453]

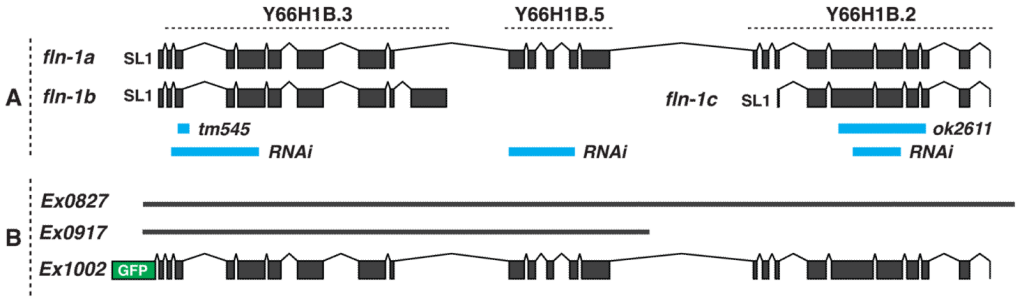

Figure 1. Gene structure of the *fln-1* locus

This figure is a diagrammatic representation of the *fln-1* locus derived from cDNA sequencing data. Rectangles and lines represent exons and introns, respectively. Solid, thick lines represent the genomic sequences. A) Predicted ORFs Y66H1B.3, Y66H1B.5, and Y66H1B.2 are indicated. Deletion alleles (*tm545* and *ok2611*) and RNAi targeting constructs are shown as blue lines. B) The rescuing constructs *Ex0827* and *Ex0917* are amplified genomic sequences, and *Ex1002* is an N-terminal GFP fusion to the *fln-1a* open reading frame. Approximately 19 kb of chromosome IV is shown.

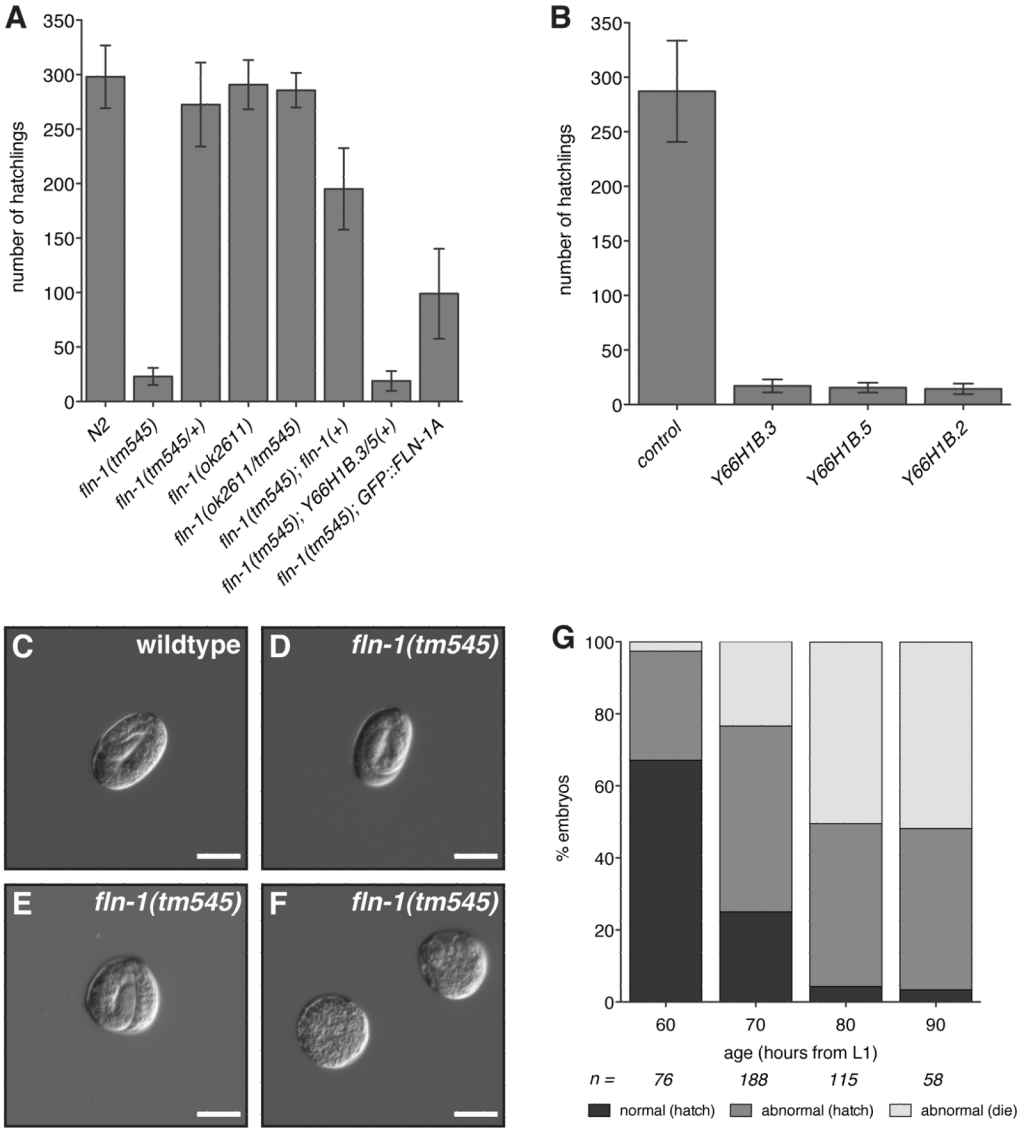

Figure 2. Filamin is required for normal brood size

A) Brood size comparison of wildtype, *fln-1* mutant and rescued animals. B) RNAi depletion of Y66H1B.3, Y66H1B.5 or Y66H1B.2 phenocopies the *tm545* brood size defect. Columns indicate the average number of hatchlings, and error bars indicate the standard deviation. C–F) wildtype animals produce wildtype, oval-shaped embryos (C). *tm545* animals initially produce normal embryos (D), but progressively worsen producing round (E), and eventually inviable embryos (F). Bar indicates 25 μm. G) Shape and hatching of *tm545* embryos was determined at the indicated maternal ages. Older *tm545* animals produce a higher proportion of misshapen and arrested embryos (G). During this time course, age-matched wildtype animals produce only normally shaped embryos, of which all hatch (n=561). Control wildtype animals are omitted from (G) for simplification. Number of *tm545* embryos examined for each time point is indicated.

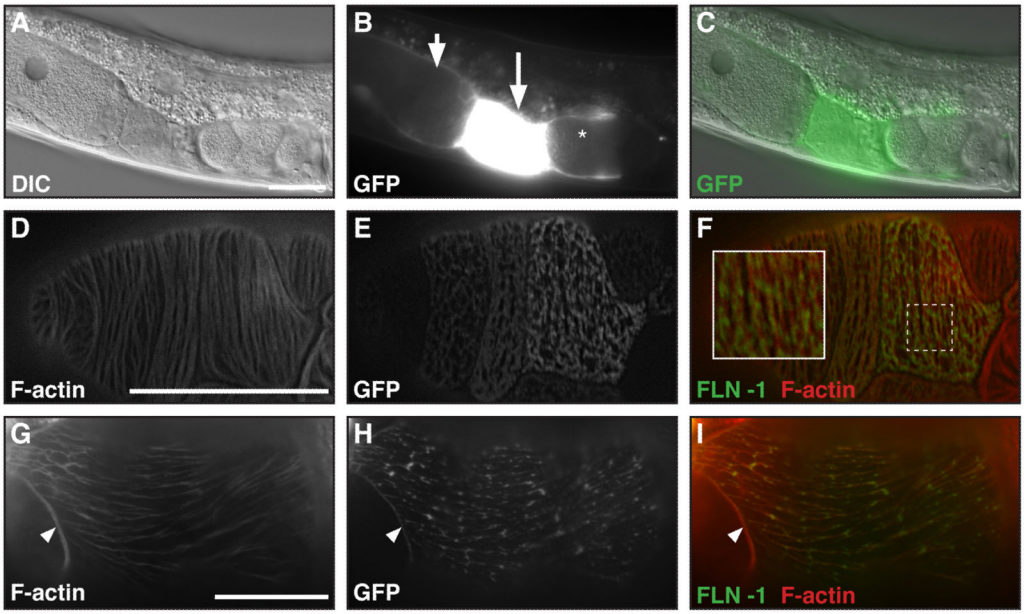

Figure 3. FLN-1 is expressed in the somatic gonad and colocalizes with F-actin

A) DIC image of an adult hermaphrodite carrying a transcriptional *fln-1::gfp* fusion, and (B) a corresponding GFP image. The *fln-1::gfp* transcriptional fusion is expressed strongly in the proximal sheath cells (arrowhead), spermatheca (arrow), and the uterus (asterisk) in adult animals. C) Merged GFP and DIC images. D–I) GFP::FLN-1A translational fusion expressed in the spermatheca (D) and uterus (G) and co-stained for F-actin (E and H). GFP::FLN-1A appears to colocalize with F-actin in the spmeratheca (F) and the uterus (I). Arrows in G–I indicate the uterine lariat. F and I) Merged F-actin (red) and GFP::FLN-1A (green). Bar indicates 25 μm.

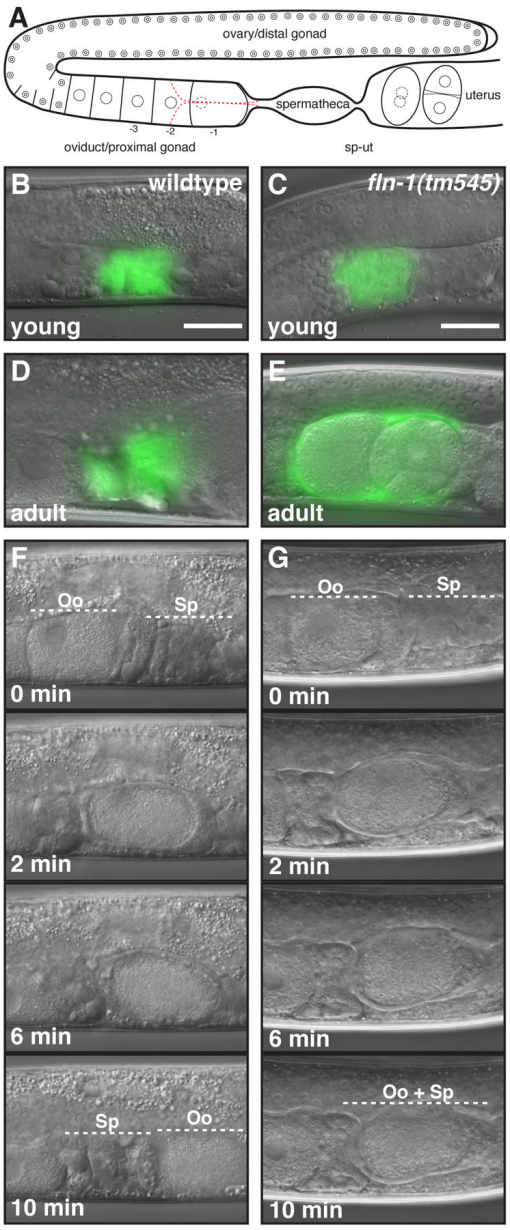

Figure 4. Ovulation time-lapse of *fln-1(tm545)* animals

A) Schematic representation of the hermaphrodite gonad. B–C) Young wildtype and *fln-1(tm545)* spermatheca marked with *fkh-6::gfp*. D–E) Adult wildtype and *fln-1(tm545)* spermatheca marked with *fkh-6::gfp*. F) Wildtype ovulation sequence captured by DIC time-lapse microscopy. G) *fln-1(tm545)* ovulation sequence is identical to the wildtype ovulation during the entry (0 min) and fertilization process (2 min), but the embryos fail to exit the spermatheca (10 min). Bar indicates 25 μm.

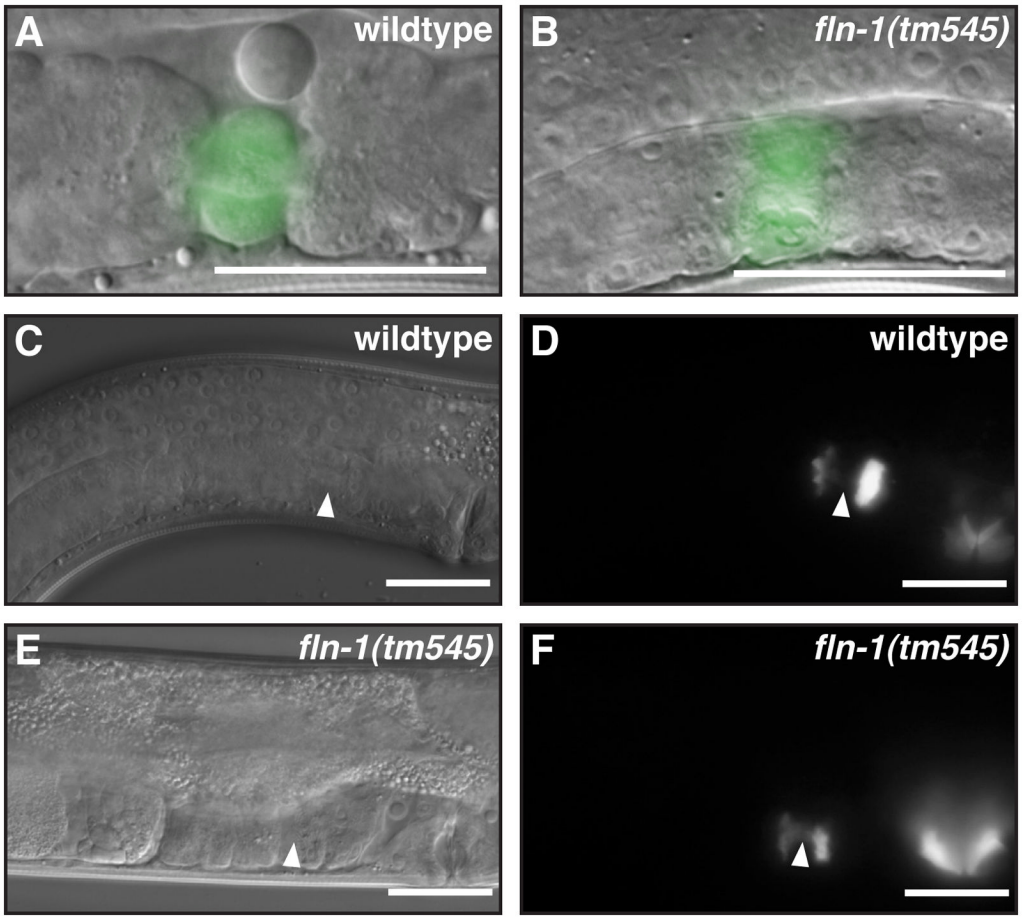

Figure 5. FLN-1 is required for normal spermatheca-uterine valve morphology

A) Wildtype sp-ut valve marked with *tag-312::gfp*. B) *fln-1(tm545)* sp-ut valve marked with *tag-312::gfp*. C–D) *cog-1::gfp* is expressed in the sujc cells (arrowheads) and in the vulva. E–F) *cog-1::gfp* is normally expressed in the sujc cells (arrowheads) of *fln-1(tm545)* animals and in the vulva. Bar indicates 25 μm.

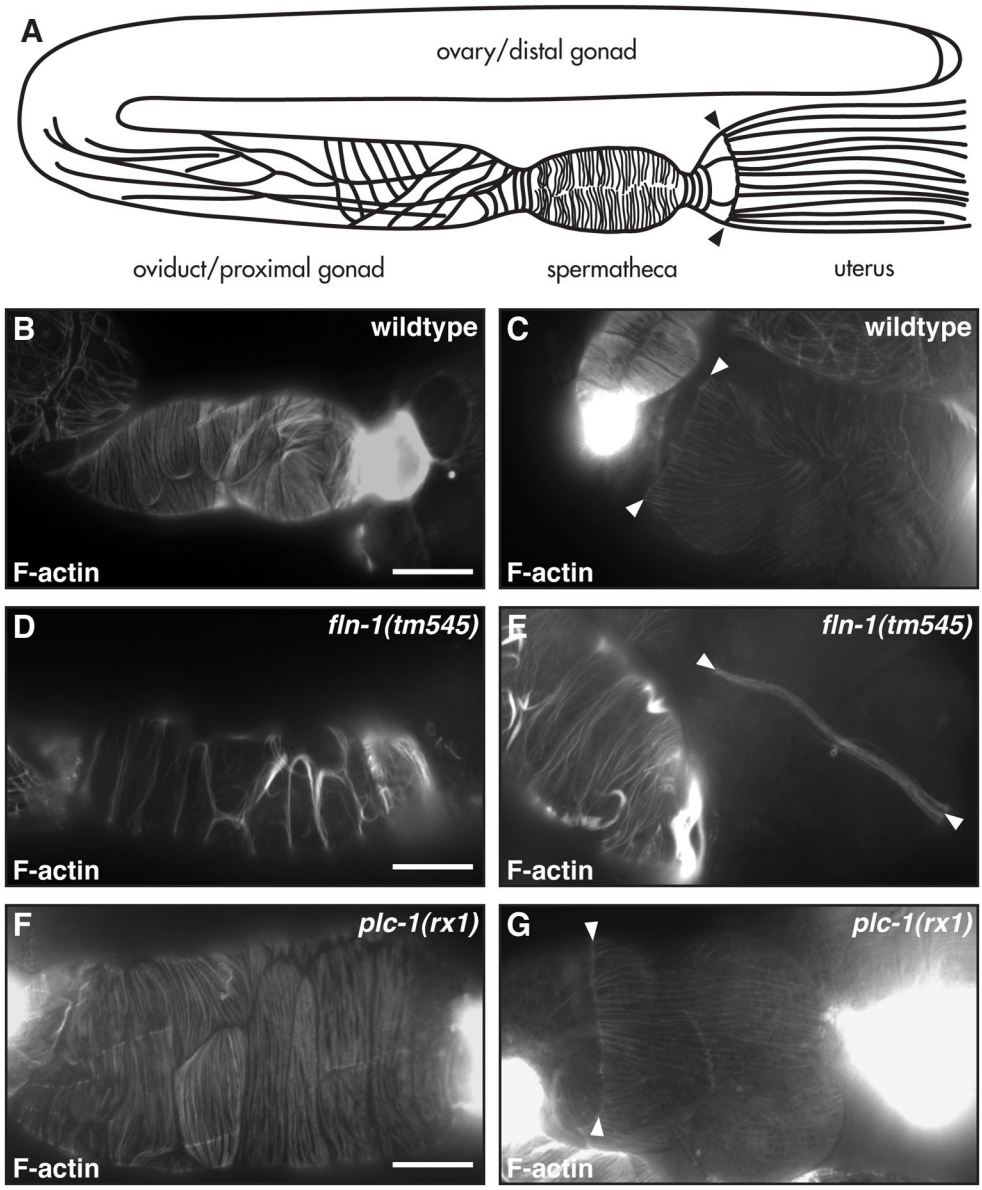

Figure 6. FLN-1 is required for maintenance of F-actin in the spermatheca and uterus

A) Diagram of F-actin in the somatic gonad. B) Wildtype spermathecal and uterine F-actin is arranged roughly circumferentially. C) Wildtype uterine actin is arranged longitudinally and originates at the uterine lariat (arrowheads). D) *fln-1(tm545)* actin is bundled into thick cortical filaments at the cell-cell junctions. E) *fln-1(tm545)* actin in the uterus appears thicker and is collapsed to the uterine lariat. F) *plc-1(rx1)* F-actin in the spermatheca is normal. G) *plc-1(rx1)* uterine lariat is normal. Arrowheads indicate the lariat. Bar indicates 25 μm.

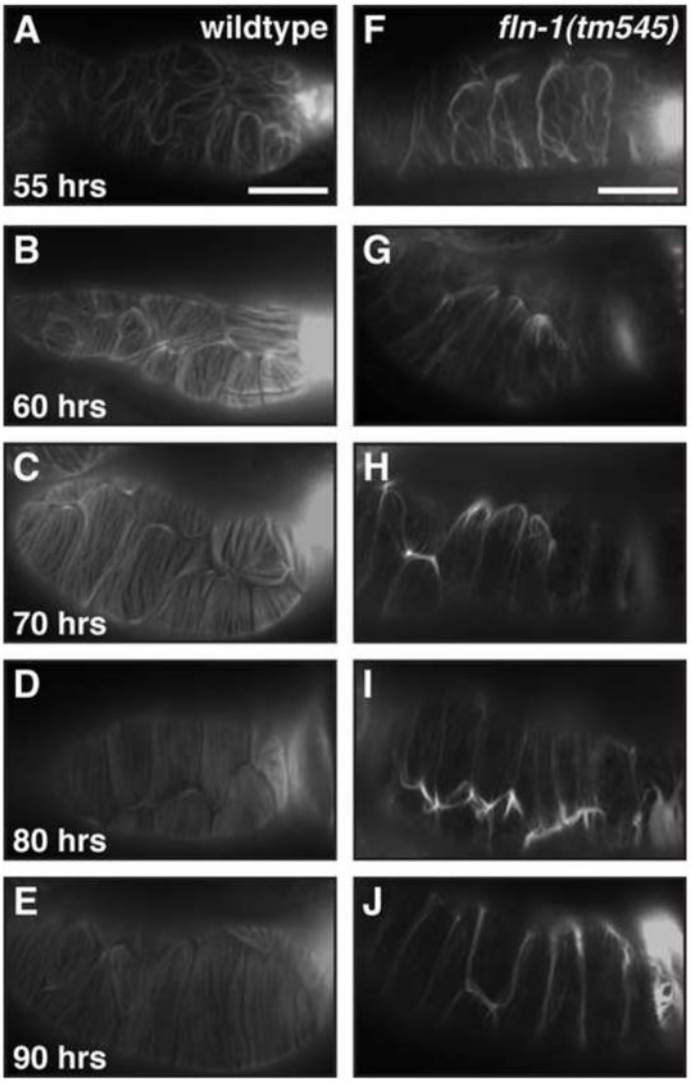

Figure 7. *fln-1(tm545)* spermathecal F-actin progressively worsens

A–E) Wildtype spermatheca F-actin at 55 (A), 60 (B), 70 (C), 80 (D), and 90 (E) hours of age. F–J) *fln-1*(tm545) F-actin at 55 (F), 60 (G), 70 (H), 80 (I), and 90 (J) hours of age. Onset of ovulation is between 55 and 60 hours, therefore (A) and (F) are before the first ovulation, while (B) and (G) are following the first ovulation. Corresponding DIC images (not shown) were used to determine number of ovulations that had occurred. Bar indicates 25 μm.